Supporting Information

Gas-to-aerosol phase partitioning of atmospheric water-soluble organic compounds at a rural site of China: An enhancing effect of NH_3 on SOA formation

Shaojun Lv[1], Fanglin Wang[1], Can Wu[1], Yubao Chen[1], Shijie Liu[1], Si Zhang[1], Dapeng Li[1], Wei Du[1], Fan Zhang[1], Hongli Wang[3], Cheng Huang[3], Qingyan Fu[4], Yusen Duan[4], Gehui Wang[1,2]*

[1]Key Lab of Geographic Information Science of the Ministry of Education, School of Geographic Sciences, East China Normal University, Shanghai 200062, China
[2] Institute of Eco-Chongming, 20 Cuiniao Rd., Chongming, Shanghai 202162, China
[3]State Environmental Protection Key Laboratory of Cause and Prevention of Urban Air Pollution Complex, Shanghai Academy of Environmental Sciences, Shanghai, 200233 China.
[4]Shanghai Environmental Monitoring Center, Shanghai 200232, China

*Corresponding author: Gehui Wang (ghwang@geo.ecnu.edu.cn)

List of supporting materials:

1. Three paragraphs describing the online measurements by the IGAC, calculation on the ALWC contributions and thermodynamic calculations on the partitioning of formic and acetic acids.
2. Two tables, Table S1-Table S2
3. Eight figures, Figure S1-Figure S8.
4. References

Detailed description of the online measurement by the IGAC and method accuracy test

Water-soluble organic compounds (WSOC) in the gas-phase (WSOCg) and $PM_{2.5}$-associated (WSOCp) were simultaneously measured with a 3-hr time resolution via an online-IC system: IGAC combined with a total organic carbon (TOC) analyzer and a total nitrogen (TN) analyzer. Fine particles ($PM_{2.5}$) were collected into aqueous samples by a scrub and impactor aerosol collector (SIC). In the front, a vertical wet annular denuder (WAD) was applied to collect the gas-phase compounds into liquid samples.[1] After determining the inorganic ions and small carboxylic acids (i.e., formic, acetic and oxalic acids), the remaining gaseous and aqueous samples were simultaneously collected every three hours and further analyzed for WSOC and water-soluble organic nitrogen (WSON) by a TOC/TON analyzer. The application of the TOC analyzer for the determination of WSOC has been described in detail elsewhere.[2] Briefly, the instrument obtains total carbon (TC) using high-temperature (680 °C) Pt-catalyzed transformation of all carbon into CO_2 coupled to nondispersive infrared (NDIR) gas detection of CO_2. The total inorganic carbon (TIC) was then measured by NDIR through conversion into CO_2 using 25% H_3PO_4. The concentrations of WSOCs are the difference between TC and TIC. Calibration curves for TC and TIC were created using $NaHCO_3$, Na_2CO_3 and potassium hydrogen phthalate standard solutions.

To test the collection efficiency of WSOCg, we chose acetic acid for comparison, as it exists abundantly in the troposphere with a relatively strong volatility and can be accurately measured by a proton transfer reaction mass spectrometer (PTR-MS, Ionicon Analytik GmbH, Austria). For IGAC, an AS18 column (2 mm × 250 mm, Dionex™ IonPac™) was used to analyze acetic acid. Detailed descriptions of PTR-MS application can be found in previous reports.[3, 4] The results are given in Figure S2a, showing that the IGAC collection efficiency of

acetic acid was on average 73%, which was similar to those of other volatile gases (e.g., formic acid and NH_3)[1, 5]. In addition to the gas-phase collection efficiency, the IGAC collection efficiency of WSOCp was also determined by comparison with filter sampling. During the entire sampling period, a total of 98 $PM_{2.5}$ samples were collected using a high-volume sampler (Tisch Environmental) with a $PM_{2.5}$ inlet at a flow rate of 1.13 m^3 min^{-1}, which was performed on a day-night basis (daytime at 08:30-19:00 and nighttime at 19:30-08:00). As shown in Figure S2b, the WSOCp concentrations measured by the IGAC collection system were similar to those of the filter, yielding an average value of 89%.

Throughout the sampling period, some gas and particle phase WSOC and inorganic species data were missing due to the electricity supply shutdown by the local government, leading to the lack of WSOC and inorganic ions data from December 17 to 24 in 2019 and January 5 to 6 in 2020.

Calculation of the contributions of the major components of $PM_{2.5}$ to ALWC

ALWC associated with inorganic species was estimated by ISORROPIA-II using meteorological conditions and the IGAC-measured inorganic compositions. The contribution of $(NH_4)_2SO_4$ was calculated by the difference between the model results without an $(NH_4)_2SO_4$ input (i.e., $(NH_4)_2SO_4$=0) and the total ALWC. Similarly, the difference in the ALWC between the predictions with and without NH_4NO_3 input showed the contribution of NH_4NO_3. The contributions of organic matter (OM) to ALWC ($ALWC_{org}$) were calculated by the following equation[6]:

$$ALWC_{org}=\frac{[OM]\rho_w}{\rho_{org}}\frac{\kappa_{org}}{\frac{1}{RH}-1} \quad (1)$$

where OM is the mass concentration of organics, ρ_w is the density of water and ρ_{org} is the density of OM (ρ_{org}=1.4 g cm^{-3}). κ_{org} is the hygroscopicity parameter of organic aerosol

composition (κ_{org}=0.06).[7]

Thermodynamic calculations of the partitioning of formic and acetic acids during the high RH period

To further elucidate the impact of NH_3 on the partitioning behavior of WSOCg in the high RH period, we conducted a thermodynamic calculation on the gas-to-aerosol partitioning of the two acids, in which S curves showing the dependence of formic and acetic acid partitioning on aerosol pH were estimated by using the following equations:

$$\varepsilon(HCOO^-)=\frac{H_{HCOOH}[ALWC]RT(\frac{\gamma_{H^+}\gamma_{HCOO^-}}{\gamma_{HCOOH}}10^{-pH}+K_{a1})\times0.987\times10^{-14}}{\gamma_{H^+}\gamma_{HCOO^-}10^{-pH}+H_{HCOOH}[ALWC]RT(\frac{\gamma_{H^+}\gamma_{HCOO^-}}{\gamma_{HCOOH}}10^{-pH}+K_{a1})\times0.987\times10^{-14}} \quad (2)$$

$$\varepsilon(CH_3COO^-)=\frac{H_{CH3COOH}[ALWC]RT(\frac{\gamma_{H^+}\gamma_{CH3COO^-}}{\gamma_{CH3COOH}}10^{-pH}+K_{a1})\times0.987\times10^{-14}}{\gamma_{H^+}\gamma_{CH3COO^-}10^{-pH}+H_{CH3COOH}[ALWC]RT(\frac{\gamma_{H^+}\gamma_{CH3COO^-}}{\gamma_{CH3COOH}}10^{-pH}+K_{a1})\times0.987\times10^{-14}} \quad (3)$$

where H_{HCOOH} and $H_{CH3COOH}$ are Henry's law constants for formic acid (9540 mol L^{-1} atm^{-1}) and acetic acid (5370 mol L^{-1} atm^{-1}).[8] R is the gas constant (8.314 m^3 Pa K^{-1} mol^{-1}), and ALWC (μg m^{-3}) and T (K) are the averages of the observed data. K_{a1} is the first acid dissociation constant of formic (1.78×10^{-4} mol L^{-1}) and acetic acid (1.75×10^{-5} mol L^{-1}).[9] γ_i are activity coefficients. γ_{HCOOH}=0.515 and $\gamma_{CH3COOH}$=3.39 were calculated using the web version of AIOMFAC, while $\gamma_{H+}\gamma_{HCOO-}=\gamma_{H+}\gamma_{CH3COO-}=\gamma_{H+}\gamma_{NO3-}$=0.235 was predicted using the E-AIM model.

As seen in Figures S6a and b, the growth trend of ambient $\varepsilon(HCOO^-)$ and $\varepsilon(CH_3COO^-)$ during the high RH period showed a strong dependence on the aerosol acidity in a pH range of 3-5, further demonstrating that the neutralization effect of NH_3 is favorable for the partitioning of WSOCg into the aerosol phase. However, the growth trends of $\varepsilon(HCOO^-)$ and $\varepsilon(CH_3COO^-)$ were underestimated by the S curves, which is similar to the results observed by

Nah et al. (2018) [9], who also reported a significant underestimation by the S curve on the partitioning of formic and acetic acids in the USA. They explained that the possible reasons for such higher-than-predicted molar fractions of aerosol-phase formic and acetic acids probably include a poor collection efficiency of the gas-phase acids, deviations of Henry's law constants from the literature values and the dimers of formic and acetic acid formation in the aerosol phase. To clarify the factors causing the underestimation, we recalculated the S curves by enlarging the Henry's law constants of formic and acetic acids by factors of 5×10^2 and 5×10^3, respectively. As shown in Figures S6c and d, the recalculated S curves can well predict the $\varepsilon(HCOO^-)$ and $\varepsilon(CH_3COO^-)$ observed on Chongming Island in the high RH period, suggesting that the enlarged Henry's law constants, which are commonly named as effective Henry's law constant, are much more realistic for illustrating the partitioning process of WSOCg in the YRD region. Documented Henry's law constants are usually determined and calculated for a pure water system. [8] However, the aqueous phase of atmospheric aerosols is a complex mixture. Thus, many species and chemical reactions can affect the WSOCg partitioning process, leading to a significant underestimation. Nevertheless, the strong dependences of $\varepsilon(HCOO^-)$ and $\varepsilon(CH_3COO^-)$ on the pH values, which were regulated by NH_3, either observed in Chongming Island or predicted by the S curves clearly demonstrate that the neutralization of NH_3 with organic acids was important under the high RH conditions, which enhanced significantly the WSOCg partitioning.

Table S1 Observed NH_3 mean concentrations (μg m^{-3}) in different regions of China.

Location	Type	Region	Period	NH_3	Reference
Gucheng	Rural	NCP	Mar.2016-May.2017	22.2±12.8 [a]	Kuang et al. (2020)[10]
Gucheng	Rural	NCP	May-Sep 2013	27.5±42.8 [a]	Meng et al. (2018)[11]
Luancheng	Farmland	NCP	Dec.2015-Feb.2016	17.2	Pan et al. (2018)[12]
Cangzhou	suburban	NCP	Dec.2015-Feb.2016	22.2	Pan et al. (2018)[12]
Lin'an	Rural	YRD	Sep 2009-Dec 2010	12.5±8.5 [a]	Meng et al. (2014)[13]
Shanghai	Rural	YRD	Dec.2019-Jan.2020	9.3±4.0	This study
Shanghai	Rural	YRD	July-Dec 2013, Mar-June 2014	9.4±6.9 [a]	Wang et al. (2015)[14]
Nanjing	Urban	YRD	Dec.2015-Feb.2016	7.5	Pan et al. (2018)[12]
Guangzhou	Urban	PRD	Dec.2015-Feb.2016	4.4	Pan et al. (2018)[12]
Guangzhou	Rural	PRD	Oct-Nov 2004	7.3±6.2	Hu et al. (2008)[15]
Maoming	Urban	PRD	Dec.2015-Feb.2016	5.9	Pan et al. (2018)[12]
Hongkong	Urban	PRD	Autumn 2000	2.3±2.7 [a]	Yao et al. (2006)[16]
Akesu	Farmland	Northwest	Dec.2015-Feb.2016	3.2	Pan et al. (2018)[12]
Cele	Desert	Northwest	Dec.2015-Feb.2016	3.1	Pan et al. (2018)[12]
Linze	farmland	Northwest	Dec.2015-Feb.2016	2.3	Pan et al. (2018)[12]

[a] The unit of NH_3 concentrations in the original text is ppb, which was converted by the formula of standard atmospheric pressure and normal temperature in this study, for example,

$$22.2\ \mu g\ m^{-3} = \frac{29.2\ ppb \times 17}{22.4}$$

Table S2 Average concentrations (μg m^{-3}) of $PM_{2.5}$, ammonium, nitrate, sulfate and WSOCp in different regions of China

Code	Location	Region	Time	$PM_{2.5}$	NH_4^+	NO_3^-	SO_4^{2-}	WSOCp	Reference
SH	Shanghai	YRD	Winter, 2019	55±40	7.0±5.5	16±14	6.0±4.1	4.6±2.9	This study
BJ	Beijing	NCP	Winter, 2016	176		39	15		Sun et al. 2019[17]
BJ	Beijing	NCP	Winter, 2016	76±70				10±10	Yang et al. 2019[18]
BJ	Beijing	NCP	Winter, 2017	61±45	8.0±6.5	16±21	6.9±6.4	7.2±5.0	Li et al. 2020[19]
TJ	Tianjin	NCP	Winter, 2011	71±60	61±45	13±13	15±16	14±12	Xu et al. 2016[20]
LC	Liaocheng	NCP	Winter, 2017	308±188	22±14	73±57	36±17	41±14	Meng et al. 2020[21]
SH	Shanghai	YRD	Summer, 2005	67±28	4.2±2.1	7.2±6.7	16±9.8	5.8±4.2	Pathak et al. 2011[22]
SH	Shanghai	YRD	Summer, 2014	30±13	8.9±4.0	4.8±3.9	8.2±4.5	3.4±1.3	Zhao et al. 2016[23]
SH	Shanghai	YRD	Winter, 2013	105±65	12±8.9	21±19	17±11	9.6±6.6	Zhao et al. 2016[23]
CZ	Changzhou	YRD	Summer, 2015	81±38	8.2±4.3	6.8±6.2	16±9.8	6.4±1.8	Ye et al. 2017[24]
CZ	Changzhou	YRD	Winter, 2015	127±50	13±3.7	24±12	19±7.6	14±6.6	Ye et al. 2017[24]
NS	Nansha	PRD	Annual 2009	44±27	5.5±3.6	4.8±4.4	12±7.2	3.9±2.5	Kuang et al. 2015[25]
GZ	Guangzhou	PRD	Annual 2009	56±30	6.8±4.2	6.7±6.3	13±6.8	4.9±2.5	Kuang et al. 2015[25]
GZ	Guangzhou	PRD	Summer, 2004	59±28	5.0±2.2	5.8±4.2	13±6.0	4.3±1.2	Pathak et al. 2011[22]
GZ	Guangzhou	PRD	Winter, 2012	75±24	5.1±2.1	5.8±3.4	11±4.4	4.1±2.0	Liu et al. 2014[26]
GZ	Guangzhou	PRD	Winter, 2016	118±26	5.5±2.2	11±8.9	9.2±3.9	5.3±2.0	Jiang et al. 2020[27]
LZ	Lanzhou	NW	Summer, 2006	65±29	3.8±2.0	2.7±2.0	11±6.0	2.4±0.80	Pathak et al. 2011[22]
QH	Qinghai	NW	Winter, 2011	44±22	0.85±0.9	2.1±1.4	5.3±5.6	1.5±0.84	Zhao et al. 2015[28]
QH	Qinghai	NW	Summer, 2012	22±14	0.73±0.7	1.3±1.3	4.5±3.5	1.3±0.38	Zhao et al. 2015[28]

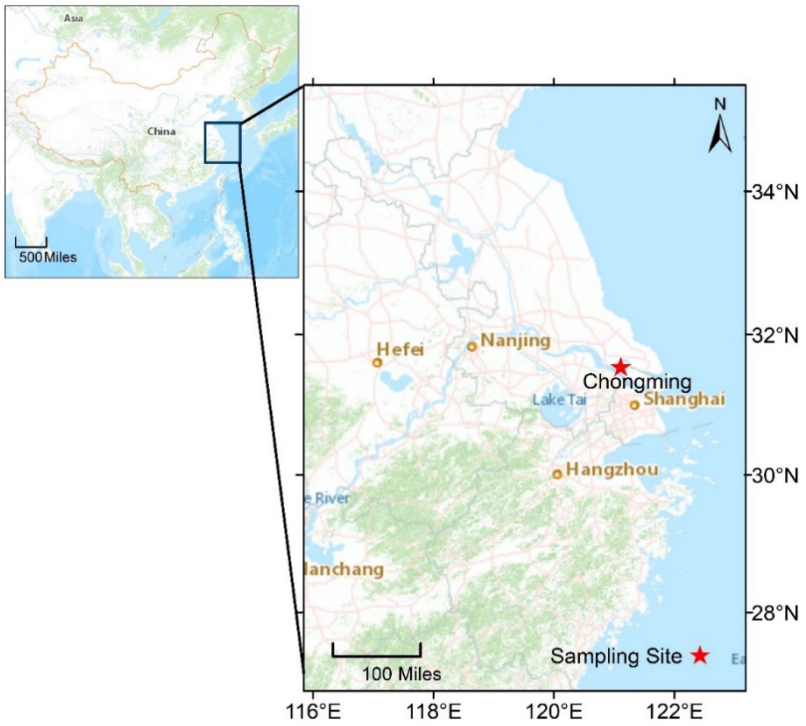

Figure S1. Geographic location of the sampling site in Chongming, China.

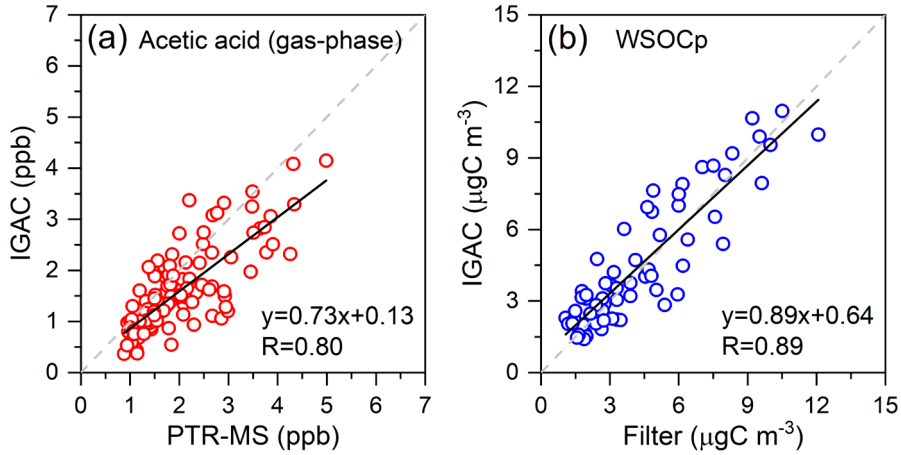

Figure S2. A comparison of species measured by IGAC and other techniques ((**a**) gas-phase acetic acid, and (**b**) fine particulate WSOC).

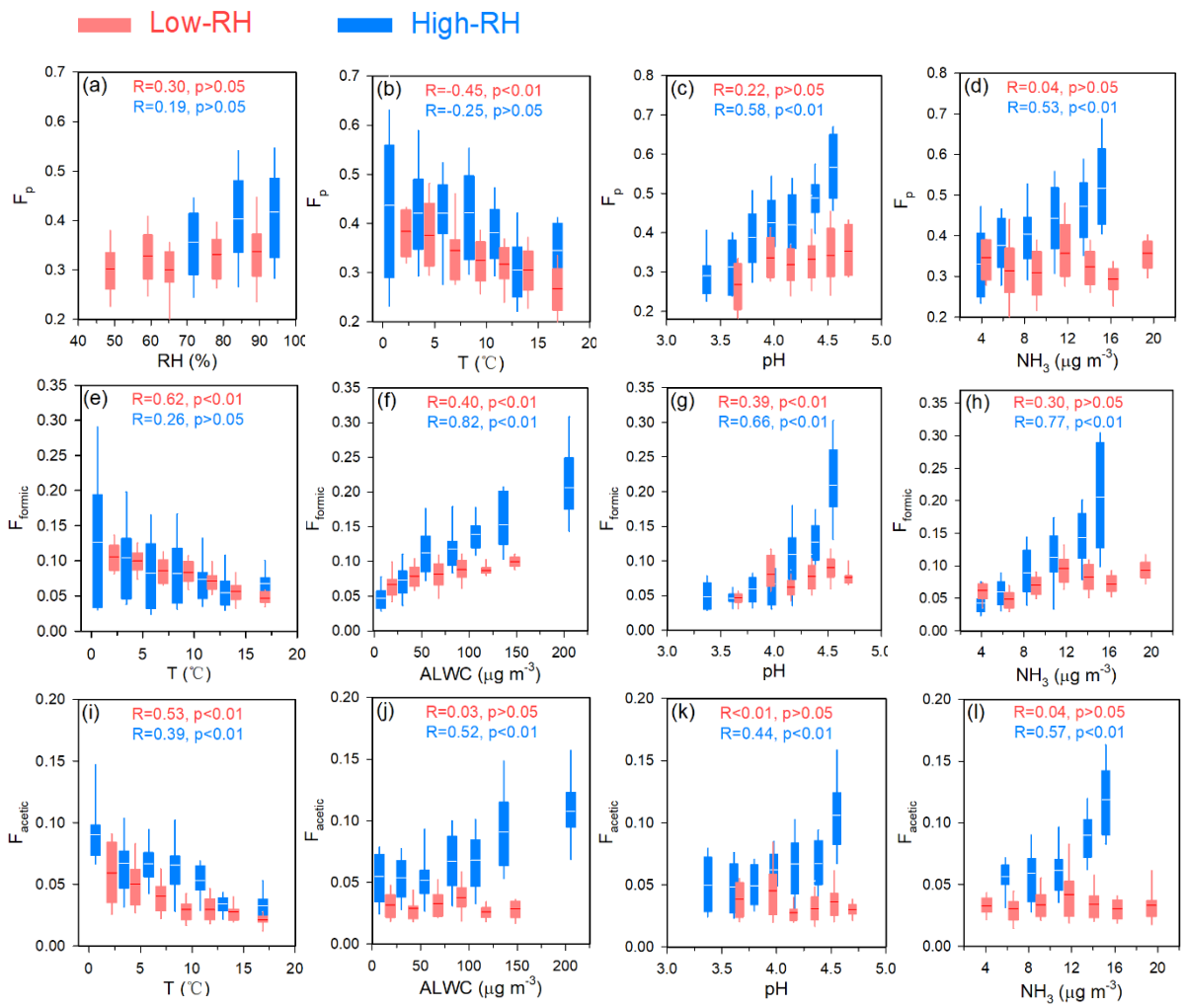

Figure S3. Factors affecting the gas-to-aerosol phase-partitioning coefficients (Fp) of WSOCg, formic acid (F_{formic}) and acetic acid (F_{acetic}) in the YRD region of China in the low and high RH periods ((**a**) relative humidity, RH; (**b**), (**e**) and (**i**) temperature, T; (**f**) and (**j**) aerosol liquid water content, ALWC; (**c**), (**g**) and (**k**) $PM_{2.5}$ acidity, pH; and (**d**), (**h**) and (**l**) NH_3 concentrations). Fp, F_{formic} or F_{acetic} $=C_p/(C_g+C_p)$, C_p and C_g are the concentrations of WSOC and formic or acetic acid in the particle phase and gas phase, respectively.

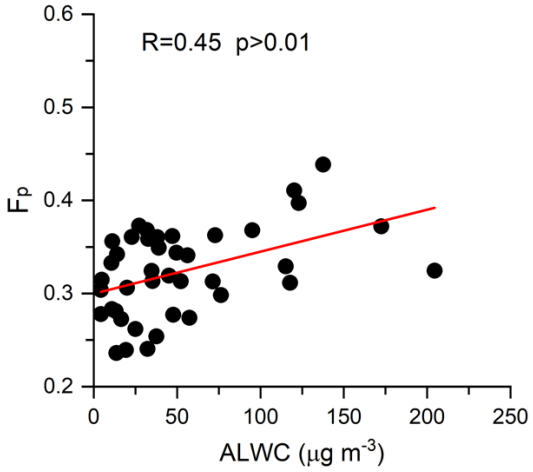

Figure S4. Linear regression fit for Fp versus ALWC of $PM_{2.5}$ in the nighttime during the low RH period with the hourly RH higher than 80%.

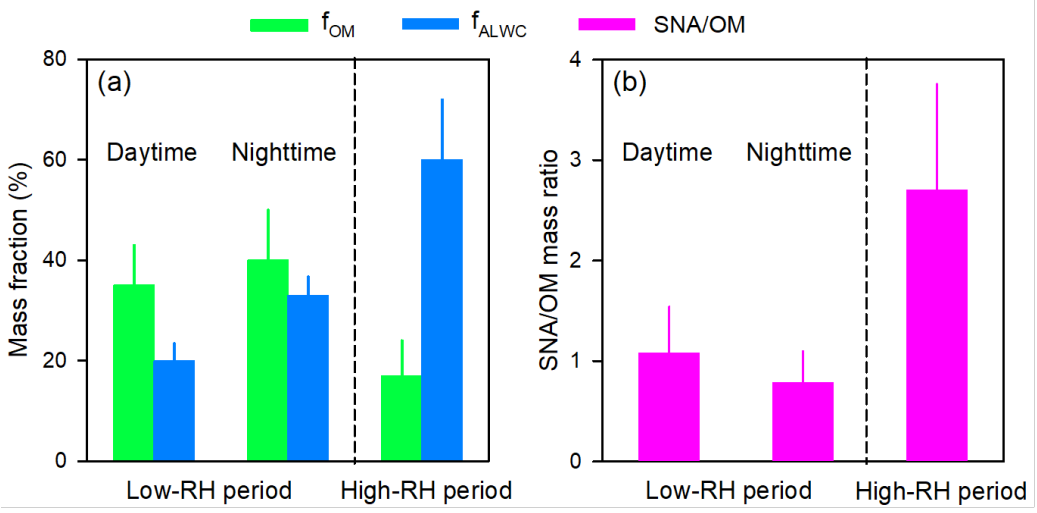

Figure S5. (a) The mass fraction of organic matter (f_{OM}=OC×1.8/(ALWC+$PM_{2.5}$)) and ALWC (f_{ALWC}=ALWC/(ALWC+$PM_{2.5}$)). **(b)** The concentration ratio of SNA to OM (SNA/OM) during the low RH and high RH periods, respectively (OM=OC×1.8).

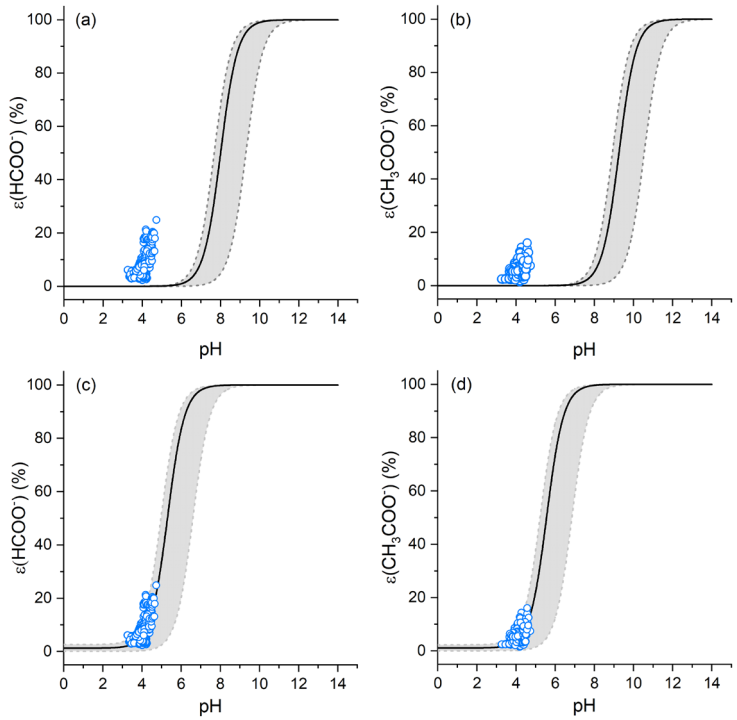

Figure S6. Analytically estimated S curves of partitioning of formic acid ε($HCOO^-$) and acetic acid ε(CH_3COO^-) (solid black lines) and ambient data (blue circles) during the high RH period. For the analytically estimated S curves, we used γ_{HCOOH}=0.515 and $\gamma_{CH3COOH}$=3.39 (AIOMFAC predicted). Similar to Nah et al. (2018),[9] we assumed that $\gamma_{H+}\gamma_{HCOO-}=\gamma_{H+}\gamma_{CH3COO-}=\gamma_{H+}\gamma_{NO3-}$=0.235, which was predicted by the E-AIM model.. The black lines are S curves calculated based on the temperature and ALWC averages (7.7 ºC and 60 μg m^{-3}, respectively) in the high RH period. The dashed lines are S curves calculated based on the minimum values (-0.9 ºC and 3.0 μg m^{-3}, respectively) and the averages plus one standard deviation (7.7±3.9 ºC and 60±69 μg m^{-3}, respectively). The S curves in (**a**) and (**b**) were calculated using the documented Henry's law constants, [29] while those in (**c**) and (**d**) were calculated by enlarging the Henry's law constants of formic and acetic acids by factors of 5×10^2 and 5×10^3, respectively.

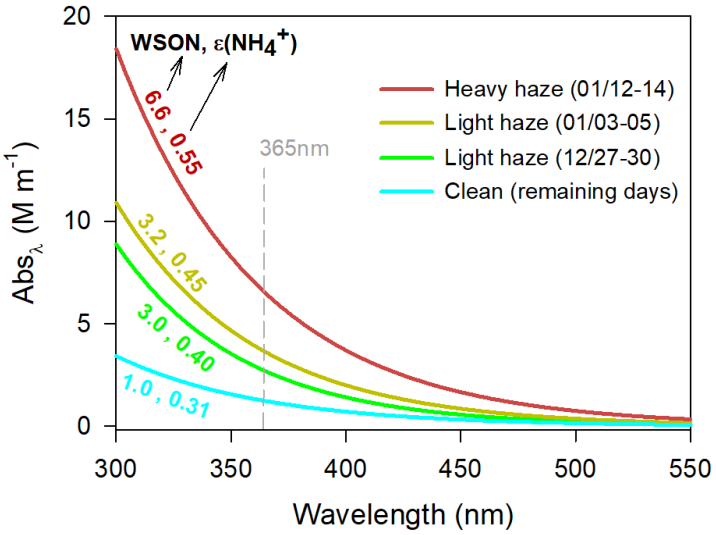

Figure S7. Average light absorption (Abs, M m^{-1}) of water extracts of $PM_{2.5}$ at wavelengths of 300-550 nm at different levels of WSON (μgN m^{-3}) and ε(NH_4^+) in the high RH period (heavy haze: daily $PM_{2.5}$>100 μg m^{-3}; light haze: 100 μg m^{-3}>daily $PM_{2.5}$>75 μg m^{-3}; and clean: daily $PM_{2.5}$<75 μg m^{-3}).

.

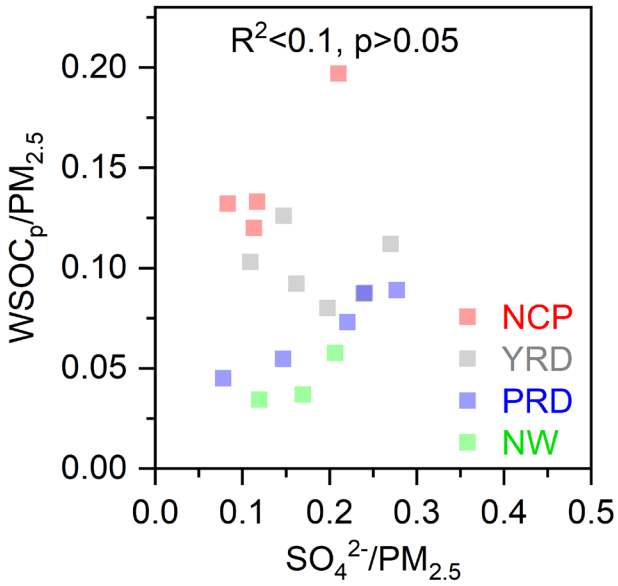

Figure S8. Scatter plots of WSOCp mass fractions vs. the relative abundances of sulfate observed at the national scale in China from the literature and this study (red, gray, blue and green colors correspond to the observation sites located on the North China Plain (NCP), YRD (Yangtze River Delta), PRD (Pearl River Delta) and Northwest (NW) China, respectively. Details of the reviewed literature are shown in Table S2).

References:

1. Young, L. H.; Li, C. H.; Lin, M. Y.; Hwang, B. F.; Hsu, H. T.; Chen, Y. C.; Jung, C. R.; Chen, K. C.; Cheng, D. H.; Wang, V. S.; Chiang, H. C.; Tsai, P. J., Field performance of a semi-continuous monitor for ambient PM2.5 water-soluble inorganic ions and gases at a suburban site. *Atmos. Environ.* **2016,** *144*, 376-388.
2. Ge, X. L.; Shaw, S. L.; Zhang, Q., Toward Understanding Amines and Their Degradation Products from Postcombustion CO2 Capture Processes with Aerosol Mass Spectrometry. *Environmental Science & Technology* **2014,** *48*, (9), 5066-5075.
3. Pan, X.; Kanaya, Y.; Tanimoto, H.; Inomata, S.; Wang, Z.; Kudo, S.; Uno, I., Examining the major contributors of ozone pollution in a rural area of the Yangtze River Delta region during harvest season. *Atmos. Chem. Phys.* **2015,** *15*, (11), 6101-6111.
4. Zhou, X.; Li, Z.; Zhang, T.; Wang, F.; Wang, F.; Tao, Y.; Zhang, X.; Wang, F.; Huang, J., Volatile organic compounds in a typical petrochemical industrialized valley city of northwest China based on high-resolution PTR-MS measurements: Characterization, sources and chemical effects. *Science of the Total Environment* **2019,** *671*, 883-896.
5. Xu, J.; Chen, J.; Shi, Y.; Zhao, N.; Qin, X.; Yu, G.; Liu, J.; Lin, Y.; Fu, Q.; Weber, R. J.; Lee, S.-H.; Deng, C.; Huang, K., First Continuous Measurement of Gaseous and Particulate Formic Acid in a Suburban Area of East China: Seasonality and Gas-Particle Partitioning. *Acs Earth and Space Chemistry* **2020,** *4*, (2), 157-167.
6. Guo, H.; Xu, L.; Bougiatioti, A.; Cerully, K. M.; Capps, S. L.; Hite, J. R.; Carlton, A. G.; Lee, S. H.; Bergin, M. H.; Ng, N. L.; Nenes, A.; Weber, R. J., Fine-particle water and pH in the southeastern United States. *Atmos. Chem. Phys.* **2015,** *15*, (9), 5211-5228.
7. Gunthe, S. S.; Rose, D.; Su, H.; Garland, R. M.; Achtert, P.; Nowak, A.; Wiedensohler, A.; Kuwata, M.; Takegawa, N.; Kondo, Y.; Hu, M.; Shao, M.; Zhu, T.; Andreae, M. O.; Poeschl, U., Cloud condensation nuclei (CCN) from fresh and aged air pollution in the megacity region of Beijing. *Atmos. Chem. Phys.* **2011,** *11*, (21), 11023-11039.
8. Sander, R., Compilation of Henry's law constants (version 4.0) for water as solvent. *Atmos. Chem. Phys.* **2015,** *15*, (8), 4399-4981.
9. Nah, T.; Guo, H. Y.; Sullivan, A. P.; Chen, Y. L.; Tanner, D. J.; Nenes, A.; Russell, A.; Ng, N. L.; Huey, L. G.; Weber, R. J., Characterization of aerosol composition, aerosol acidity, and organic acid partitioning at an agriculturally intensive rural southeastern US site. *Atmospheric Chemistry and Physics* **2018,** *18*, (15), 11471-11491.
10. Kuang, Y.; Xu, W. Y.; Lin, W. L.; Meng, Z. Y.; Zhao, H. R.; Ren, S. X.; Zhang, G.; Liang, L. L.; Xu, X. B., Explosive morning growth phenomena of NH3 on the North China Plain: Causes and potential impacts on aerosol formation. *Environmental Pollution* **2020,** *257*.
11. Meng, Z. Y.; Xu, X. B.; Lin, W. L.; Ge, B. Z.; Xie, Y. L.; Song, B.; Jia, S. H.; Zhang, R.; Peng, W.; Wang, Y.; Cheng, H. B.; Yang, W.; Zhao, H. R., Role of ambient ammonia in particulate ammonium formation at a rural site in the North China Plain. *Atmos. Chem. Phys.* **2018,** *18*, (1), 167-184.
12. Pan, Y. P.; Tian, S. L.; Zhao, Y. H.; Zhang, L.; Zhu, X. Y.; Gao, J.; Huang, W.; Zhou, Y. B.; Song, Y.; Zhang, Q.; Wang, Y. S., Identifying Ammonia Hotspots in China Using a National Observation Network. *Environmental Science & Technology* **2018,** *52*, (7), 3926-3934.
13. Meng, Z.; Zhang, R.; Lin, W.; Jia, X.; Yu, X.; Yu, X.; Wang, G., Seasonal Variation of Ammonia and Ammonium Aerosol at a Background Station in the Yangtze River Delta Region, China. *Aerosol and Air Quality Research* **2014,** *14*, (3), 756-766.
14. Wang, S. S.; Nan, J. L.; Shi, C. Z.; Fu, Q. Y.; Gao, S.; Wang, D. F.; Cui, H. X.; Saiz-Lopez, A.; Zhou, B., Atmospheric ammonia and its impacts on regional air quality over the megacity of Shanghai, China. *Scientific Reports* **2015,** *5*.
15. Hu, M.; Wu, Z.; Slanina, J.; Lin, P.; Liu, S.; Zeng, L., Acidic gases, ammonia and water-soluble ions in PM2.5 at a coastal site in the Pearl River Delta, China. *Atmos. Environ.* **2008,** *42*, (25), 6310-6320.

16. Yao, X.; Ling, T. Y.; Fang, M.; Chan, C. K., Comparison of thermodynamic predictions for in situ pH in PM2.5. *Atmos. Environ.* **2006,** *40*, (16), 2835-2844.
17. Sun, Z.; Duan, F.; He, K.; Du, J.; Zhu, L., Sulfate-nitrate-ammonium as double salts in PM2.5: Direct observations and implications for haze events. *Science of the Total Environment* **2019,** *647*, 204-209.
18. Yang, S.; Duan, F.; Ma, Y.; He, K.; Zhu, L.; Ma, T.; Ye, S.; Li, H.; Huang, T.; Kimoto, T., Haze formation indicator based on observation of critical carbonaceous species in the atmosphere. *Environmental Pollution* **2019,** *244*, 84-92.
19. Li, X. R.; Yang, Y.; Liu, S. Q.; Zhao, Q.; Wang, G. H.; Wang, Y. S., Light absorption properties of brown carbon (BrC) in autumn and winter in Beijing: Composition, formation and contribution of nitrated aromatic compounds. *Atmos. Environ.* **2020,** *223*.
20. Xu, W.; Fu Tzung, M.; Chen, J.; Tian, H., Ground-Based Measurement and Variation Analysis of Carbonaceous Aerosols in Wuqing. *Acta Scientiarum Naturalium Universitatis Pekinensis* **2016,** *52*, (3), 409-419.
21. Meng, J. J.; Liu, X. D.; Hou, Z. F.; Yi, Y. N.; Yan, L.; Li, Z.; Cao, J. J.; Li, J. J.; Wang, G. H., Molecular characteristics and stable carbon isotope compositions of dicarboxylic acids and related compounds in the urban atmosphere of the North China Plain: Implications for aqueous phase formation of SOA during the haze periods. *Science of the Total Environment* **2020,** *705*.
22. Pathak, R. K.; Wang, T.; Ho, K. F.; Lee, S. C., Characteristics of summertime PM2.5 organic and elemental carbon in four major Chinese cities: Implications of high acidity for water-soluble organic carbon (WSOC). *Atmos. Environ.* **2011,** *45*, (2), 318-325.
23. Zhao, M. F.; Qiao, T.; Li, Y. L.; Tang, X. X.; Xiu, G. L.; Yu, J. Z., Temporal variations and source apportionment of Hulis-C in PM2.5 in urban Shanghai. *Science of the Total Environment* **2016,** *571*, 18-26.
24. Ye, Z. L.; Liu, J. S.; Gu, A. J.; Feng, F. F.; Liu, Y. H.; Bi, C. L.; Xu, J. Z.; Li, L.; Chen, H.; Chen, Y. F.; Dai, L.; Zhou, Q. F.; Ge, X. L., Chemical characterization of fine particulate matter in Changzhou, China, and source apportionment with offline aerosol mass spectrometry. *Atmos. Chem. Phys.* **2017,** *17*, (4), 2573-2592.
25. Kuang, B. Y.; Lin, P.; Huang, X. H. H.; Yu, J. Z., Sources of humic-like substances in the Pearl River Delta, China: positive matrix factorization analysis of PM2.5 major components and source markers. *Atmos. Chem. Phys.* **2015,** *15*, (4), 1995-2008.
26. Liu, J. W.; Li, J.; Zhang, Y. L.; Liu, D.; Ding, P.; Shen, C. D.; Shen, K. J.; He, Q. F.; Ding, X.; Wang, X. M.; Chen, D. H.; Szidat, S.; Zhang, G., Source Apportionment Using Radiocarbon and Organic Tracers for PM2.5 Carbonaceous Aerosols in Guangzhou, South China: Contrasting Local- and Regional-Scale Haze Events. *Environmental Science & Technology* **2014,** *48*, (20), 12002-12011.
27. Jiang, H.; Li, J.; Chen, D.; Tang, J.; Cheng, Z.; Mo, Y.; Su, T.; Tian, C.; Jiang, B.; Liao, Y.; Zhang, G., Biomass burning organic aerosols significantly influence the light absorption properties of polarity-dependent organic compounds in the Pearl River Delta Region, China. *Environment international* **2020,** *144*, 106079-106079.
28. Zhao, Z.; Cao, J.; Shen, Z.; Huang, R.-J.; Hu, T.; Wang, P.; Zhang, T.; Liu, S., Chemical composition of PM2.5 at a high-altitude regional background site over Northeast of Tibet Plateau. *Atmospheric Pollution Research* **2015,** *6*, (5), 815-823.
29. Staudinger, J.; Roberts, P. V., A critical review of Henry's law constants for environmental applications. *Critical Reviews in Environmental Science and Technology* **1996,** *26*, (3), 205-297.